



Nanoscale

High-Throughput Force Measurement of Individual Kinesin-1 Motors during Multi-Motor Transport

Journal:	<i>Nanoscale</i>
Manuscript ID	NR-ART-03-2022-001701.R2
Article Type:	Paper
Date Submitted by the Author:	08-Aug-2022
Complete List of Authors:	Shukla, Saurabh; University of Washington Troitskaia, Alice ; University of Illinois at Urbana-Champaign, Biophysics Swarna, Nikhila; University of Illinois at Urbana-Champaign, Physics Maity, Barun; University of Illinois at Urbana-Champaign, Physics Tjioe, Marco; Element Biosciences Bookwalter, Carol; University of Vermont, Department of Biophysics Trybus, Kathleen; University of Vermont, Department of Biophysics Chemla, Yann; University of Illinois, Urbana-Champaign, Physics Selvin, Paul; University of Illinois, Center for Biophysics and Computational Biology, Physics Department

SCHOLARONE™
Manuscripts

High-Throughput Force Measurement of Individual Kinesin-1 Motors during Multi-Motor Transport

Saurabh Shukla^{1,2}, Alice Troitskaia³, Nikhila Swarna^{4†}, Barun Kumar Maity^{2,4}, Marco Tjioe^{2,3,4††}, Carol S Bookwalter⁵, Kathleen M Trybus⁵, Yann R Chemla^{2,3,4}, Paul R Selvin^{2,3,4*}

¹Department of Chemical and Biomolecular Engineering, University of Illinois at Urbana-Champaign, Urbana, Illinois

²Center for the Physics of Living Cells, University of Illinois at Urbana-Champaign, Urbana, Illinois

³Center for Biophysics and Quantitative Biology, University of Illinois at Urbana-Champaign, Urbana, Illinois

⁴Department of Physics, University of Illinois at Urbana-Champaign, Urbana, Illinois

⁵Department of Molecular Physiology and Biophysics, University of Vermont, Burlington, VT

†Current address: Department of Biochemistry and Molecular Biophysics, California Institute of Technology

††Current address: Element Biosciences, San Diego, CA 92121

*To whom correspondence should be addressed: selvin@illinois.edu

Abstract

Molecular motors often work in teams to move a cellular cargo. Yet measuring the forces exerted by each motor is challenging. Using a sensor made with denatured ssDNA and multi-color fluorescence, we measured picoNewtons of forces and nanometer distances exerted by individual constrained kinesin-1 motors acting together while driving a common microtubule *in vitro*. We find that kinesins primarily exerted less than 1 pN force, even while the microtubule is bypassing artificial obstacles of 20-100 nanometer size. Occasionally, individual forces increase upon encountering obstacles, although at other times they do not, with the cargo continuing in a directional manner. Our high-throughput technique, which can measure forces by many motors simultaneously, is expected to be useful for many different types of molecular motors.

Introduction

Molecular motors produce mechanical forces to transport cargoes inside the cell. Motors are vital for many cellular processes such as cell division, cell growth, and distribution of cellular resources [1,2]. Multiple molecular motors can attach to a single cargo [3,4] and dynamically coordinate their forces with each other to move cargoes to their destination [5,6]. Frequently, motors must overcome cellular roadblocks, such as other filaments, other motors, or other proteins (e.g., tau, a microtubule-associated protein (MAP)[7,8]). Single-molecule fluorescence assays can quantify the position, run lengths, and velocities of the cargo but have not been able to determine the force generation of each motor as it participates in multi-motor transport.

Optical traps are a single molecule technique that is sensitive to forces and have been widely used to study the responses of molecular motors to applied forces [9–11], including stall forces [12–14]. Optical traps can characterize the collective force-response of multiple motors that are attached to

a single microsphere, but they cannot quantify forces by individual motors in this configuration^[12,15]. Additionally, optical traps also suffer from low throughput as data acquisition is done one at a time. On the other hand, several single-molecule force sensing techniques have been developed with DNA-based designs for increasing the throughput of force measurement^[16–24].

Here, we develop a Force Sensing by Individual Motors (FSIM) assay to directly measure forces of individual kinesins as they collectively move a common cargo while measuring the displacement and velocity of the common cargo, and we do so in high-throughput measurements of forces. Specifically, we have used a mammalian kinesin-1 motor for our study (referred to as kinesin; see methods section “Kinesin Purification”). Individual kinesins are fluorescently labeled and each one is attached to a coverslip surface through a denatured single-stranded DNA molecule. Multiple kinesins can then bind to and move a microtubule (Fig. 1a). The DNA acts as a (calibrated) spring whose length is proportional to the force which arises when a kinesin attaches to a cargo and pulls it. The nanometric displacement and velocity of the fluorescently labeled microtubule are also measured. The assay provides high-throughput measurements of forces by measuring tens to hundreds of kinesins on a single microscope movie. The technique is expected to be useful with other types of molecular motors such as myosin and dynein. Our assay enables force resolution at the single motor level during collective cargo transport, a task that is difficult to achieve with conventional assays.

Results

Design of FSIM assay

The FSIM assay was closely based on our previous publication where we measured the displacement of multiple kinesins held down independently to a coverslip as they simultaneously moved a common microtubule cargo^[6] (see Fig. 1a). The displacement of individual kinesins was measured by localizing a quantum dot attached to the end of kinesin which was placed on the coverslip via a flexible double-stranded DNA (dsDNA) molecule. To measure the force exerted by the kinesins, we needed a reliable “spring” of known elastic behavior to convert the displacement, x , into a force F . We found that dsDNA was *not* an effective force-sensing molecule at high forces; small errors in measured extension (determined by imaging) translated into large errors in force calculation (Fig. S1).

In contrast, we found that denatured single-stranded DNA (ssDNA_{DEN}) worked well in the range of 0–15 pN (Fig. 1a). Denaturation of the ssDNA with glyoxal was necessary to eliminate any secondary structures which can cause instantaneous discontinuities in the force-extension behavior when pulling^[25]. By attaching the quantum dot labeled kinesins that were placed on the surface reasonably sparsely, the kinesin motors were placed sufficiently far away from each other such that no two kinesins were in the same diffraction-limited spot. We optimized our experimental protocol such that one quantum dot was attached to one kinesin and one ssDNA_{DEN} molecule to ensure the accuracy of our force measurement (see methods). Kinesin with biotin on its C-terminal was mixed with an excess amount of streptavidin labeled quantum dots. We used our in-house

developed Magnetic Cytoskeleton Affinity purification (MiCA) purification method^[26] for purifying quantum dot (QD)-bound kinesins from free quantum dots (see methods). The biotin end of the ssDNA_{DEN} was attached to the kinesin-QD (Figure 1a), and the digoxigenin end was attached to the anti-digoxigenin antibodies present on the glass coverslip surface.

We also performed controls to minimize the non-specific binding of free quantum dots and free kinesins on the surface (See details in supplementary text S1). We did not observe any movement of microtubules without the presence of visible kinesin motors, which indicated the absence of unlabeled kinesin motors in our assay. This was possible because of MiCA purification of labeled kinesins^[26]. We labeled kinesins, microtubules, and the roadblocks (introduced later in the paper) with QD705, Hilyte 488, and QD605, respectively. Since these labeled tags were spectrally different, we could simultaneously image kinesins, roadblocks, and microtubules in three different cameras (Fig. 1b). Owing to the high photostability of quantum dots and the high labeling density of microtubules, we could image for several minutes (>5 minutes) to collect force data of hundreds of kinesins per movie.

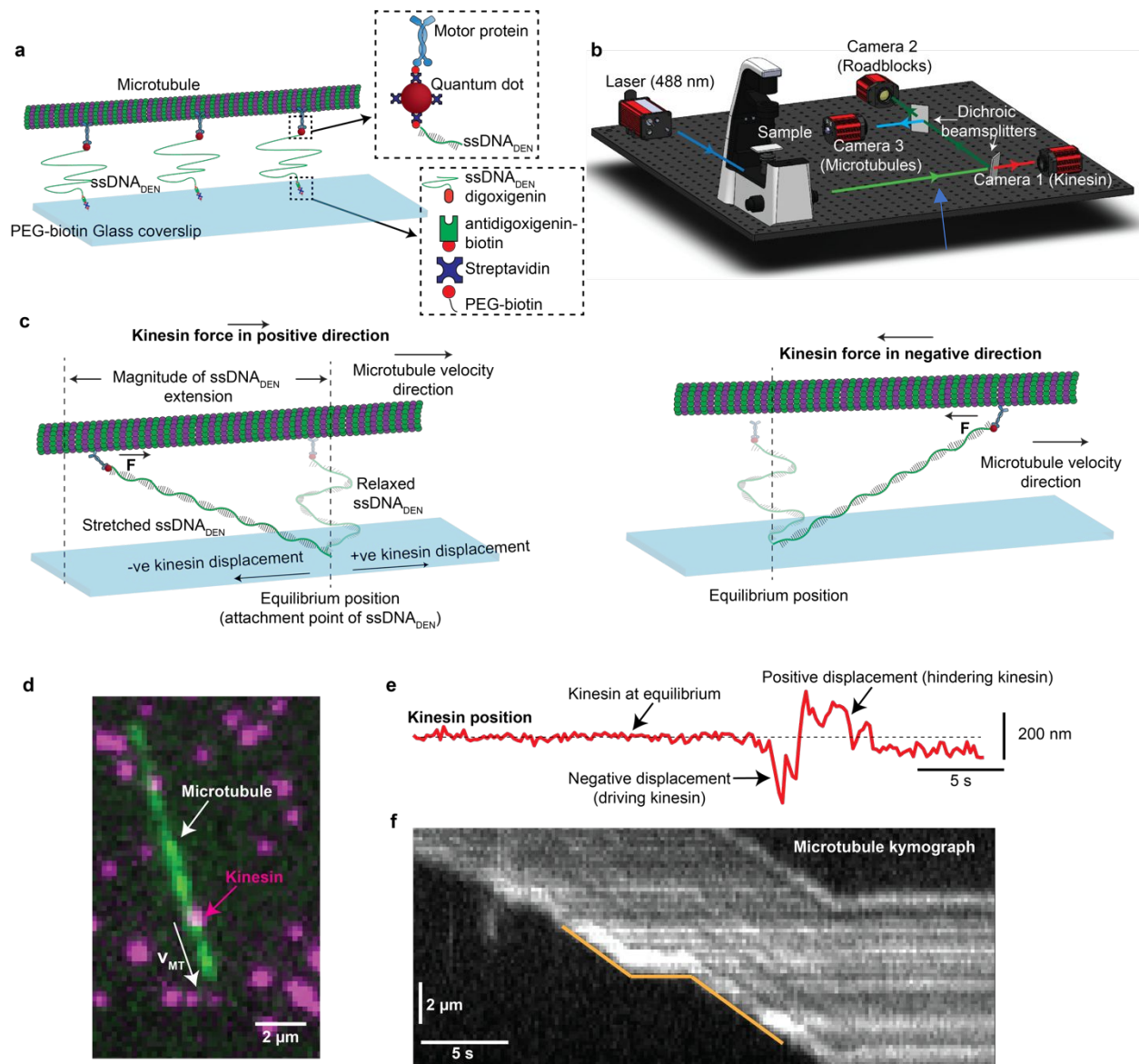


Figure 1 | Design of the FSIM assay. (a) Configuration of our FSIM assay where multiple kinesins can simultaneously transport a common microtubule. Kinesins are attached to the surface using a ssDNA_{DEN} linker and are placed sufficiently away from each other to be tracked individually. (b) Schematic of the microscope setup where the signal from kinesins, microtubules, and the roadblocks can be captured in three separate cameras. We label kinesins (with QD705), microtubule (with Hilyte 488), and the roadblocks (with QD605) with spectrally different fluorescent tags. (c) The Schematic depicts the force calculation procedure for individual kinesins. The microtubule velocity direction is shown by the arrow. Kinesin walks on the microtubule in the negative direction and thus propelling the microtubule in the position direction. By convention, displacements in the direction of the microtubule velocity are assumed to be positive displacements. Kinesin exerts force in the positive direction (direction of the microtubule velocity) when it has negative displacement (left schematic). ssDNA_{DEN} extends when kinesin starts producing force after encountering the microtubule. Kinesin force is calculated from the ssDNA_{DEN} extension as determined from the fluorescent signal of the quantum dot. The right schematic shows the kinesin molecule exerting force in the backward direction. (d) Microscope image of a microtubule (green) driven by two kinesins (magenta). The white arrow represents the direction of microtubule velocity. (e) The position of a kinesin molecule along the microtubule axis is shown. The black arrows depict the equilibrium position, positive displacements, and negative displacements. The forces of individual kinesins are derived from their displacements around the equilibrium position. (f) Kymograph of

the microtubule being driven by surface kinesins. The velocity of the microtubule is calculated by tracing the kymographs (see yellow tracing lines).

To demonstrate the functionality of our force sensor, we observed microtubule transport by ssDNA_{DEN}-linked kinesin motors. Due to the stretchability of ssDNA_{DEN}, kinesins could be displaced from the attachment point of the ssDNA_{DEN} (defined as the equilibrium point of the kinesin). A kinesin could translocate in either direction (parallel or opposite to the microtubule velocity) with respect to its equilibrium position and assume a driving or hindering state (Fig. 1c) during cargo transport. In the driving state, kinesin translocated in the opposite direction of the microtubule velocity (negative displacement) and applied a positive force for propelling the microtubule in the forward direction (Fig. 1c left schematic). In the hindering state, kinesin translocated in the direction of the microtubule velocity (positive displacement) and applied a negative force (in the opposite direction of the microtubule velocity; Fig. 1c right schematic and Fig. S4).

Fig. 1d shows a microscope image of kinesins held down via ssDNA_{DEN} to the coverslip and a microtubule. We tracked the positions of individual kinesins with time. Fig. 1e shows the position trace of one of the kinesins where its equilibrium, driving, and hindering position can be seen. Kinesins remained at their equilibrium point in the absence of microtubules (dashed horizontal line). When a microtubule approached the kinesins, the kinesins were displaced from their equilibrium point as they walked on the microtubule, thereby stretching the ssDNA_{DEN}. Hence, the force exerted by each kinesin could be estimated based on the ssDNA_{DEN} extension. We note that the vertical distance between kinesin and the surface was expected to be small (38 nm, see supplementary text S2) and contributed minimally to the extension of ssDNA_{DEN} (contour length of ssDNA_{DEN} is 500 nm) and the force. Therefore, the displacement of each kinesin from its equilibrium position was assumed to be equal to the ssDNA_{DEN} extension. We also tracked the microtubule position in a different camera and calculated the microtubule's velocity by manually tracing its kymograph (Fig. 1f).

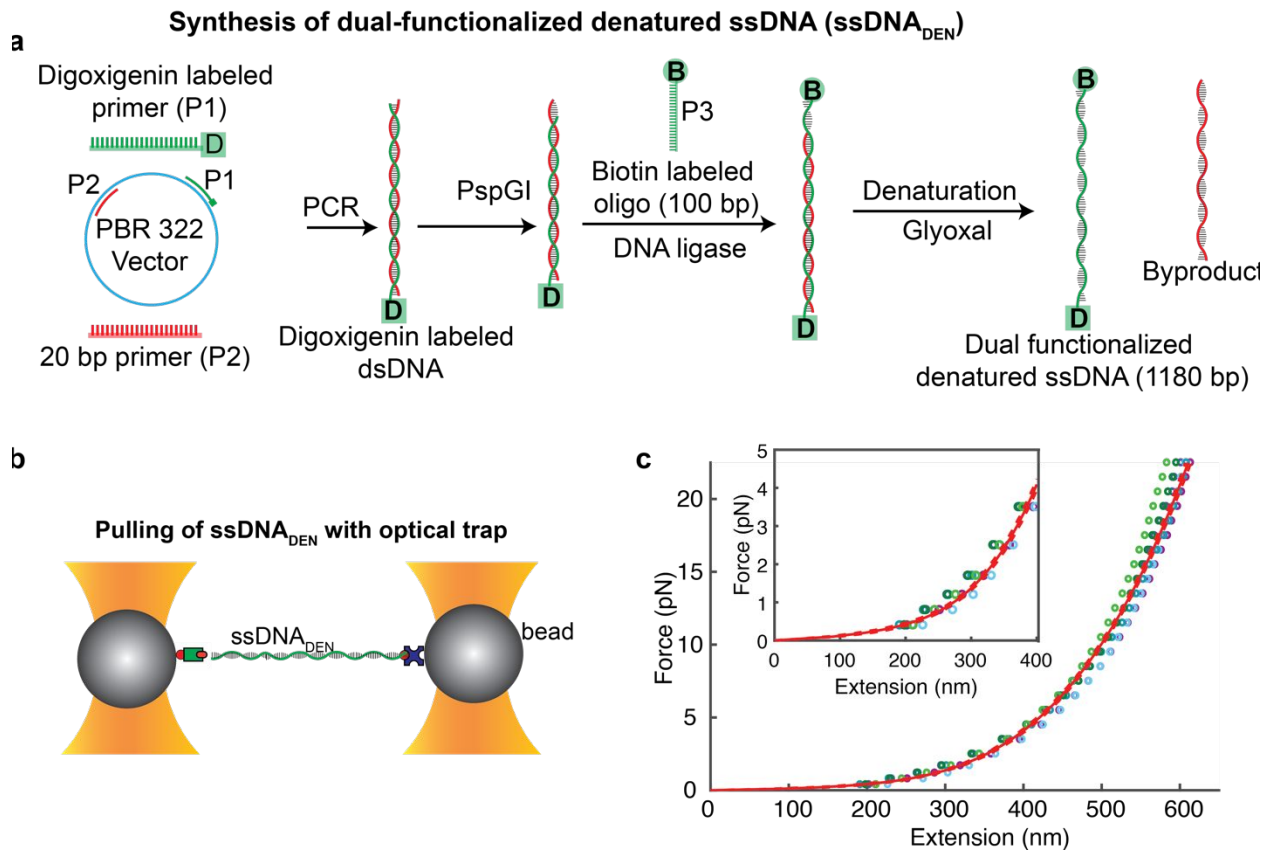


Figure 2 | Synthesis and characterization of $ssDNA_{DEN}$. (a) Synthesis of monodisperse $ssDNA_{DEN}$ functionalized with biotin at one end and digoxigenin at the other end. Glyoxal is used to synthesize denatured ssDNA ($ssDNA_{DEN}$) and to ensure minimal secondary structure formation. (b) Schematic of the optical trap assay for experimentally determining the force-extension curve of the $ssDNA_{DEN}$. (c) Force-extension curves were obtained from the optical trap assay. Colored symbols denote average force-extension curves from independent sets of measurements obtained from separate bead pairs as described in Methods; errors are smaller than marker size. These force-extension curves are fitted with an analytical model (red lines; dashed lines very close to fit are 95% confidence intervals for fit). This reference force-extension curve is used to determine the forces of individual kinesins from their respective displacements. A zoomed-in view of the model at low forces is also shown.

Synthesis and force-extension characterization of $ssDNA_{DEN}$

For the experimental realization of our assay, we needed a dual-functionalized single-stranded DNA. We synthesized monodisperse dsDNA with one strand functionalized with biotin at one end and with digoxigenin at the other end (Fig. 2a and Methods). Subsequently, we denatured the dsDNA with glyoxal and obtained our desired 1180 bp long $ssDNA_{DEN}$ product. Glyoxal covalently binds to the DNA base pairs and prevents secondary structures, making the $ssDNA_{DEN}$ a reliable construct for force sensing applications^[25,27].

We characterized the force-extension characteristics of our $ssDNA_{DEN}$ molecule using an optical trap assay (Fig. 2b). We pulled on individual $ssDNA_{DEN}$ molecules using dual-trap optical tweezers^[28,29] where a $ssDNA_{DEN}$ -coated streptavidin microsphere was captured in one trap and a microsphere coated with anti-digoxigenin antibody in the other. We obtained force-extension

curves (FECs) of ssDNA_{DEN} molecules in the same imaging buffer used for fluorescence measurements. The majority of force-extension curves (Fig. 2c and S5) fit well to an analytical expression based on previously published data^[27,30] (see methods). We used the obtained analytical expression as our reference model for calculating the forces of kinesin motors in our force-sensing assay (Fig. 2c). Unlike the force-extension curve of dsDNA, the ssDNA_{DEN} curve has a moderate slope that makes our ssDNA_{DEN} construct a more sensitive and reliable force sensing molecule for molecular motors in the relevant force range of 0-10 pN (Fig. 2c and S1).

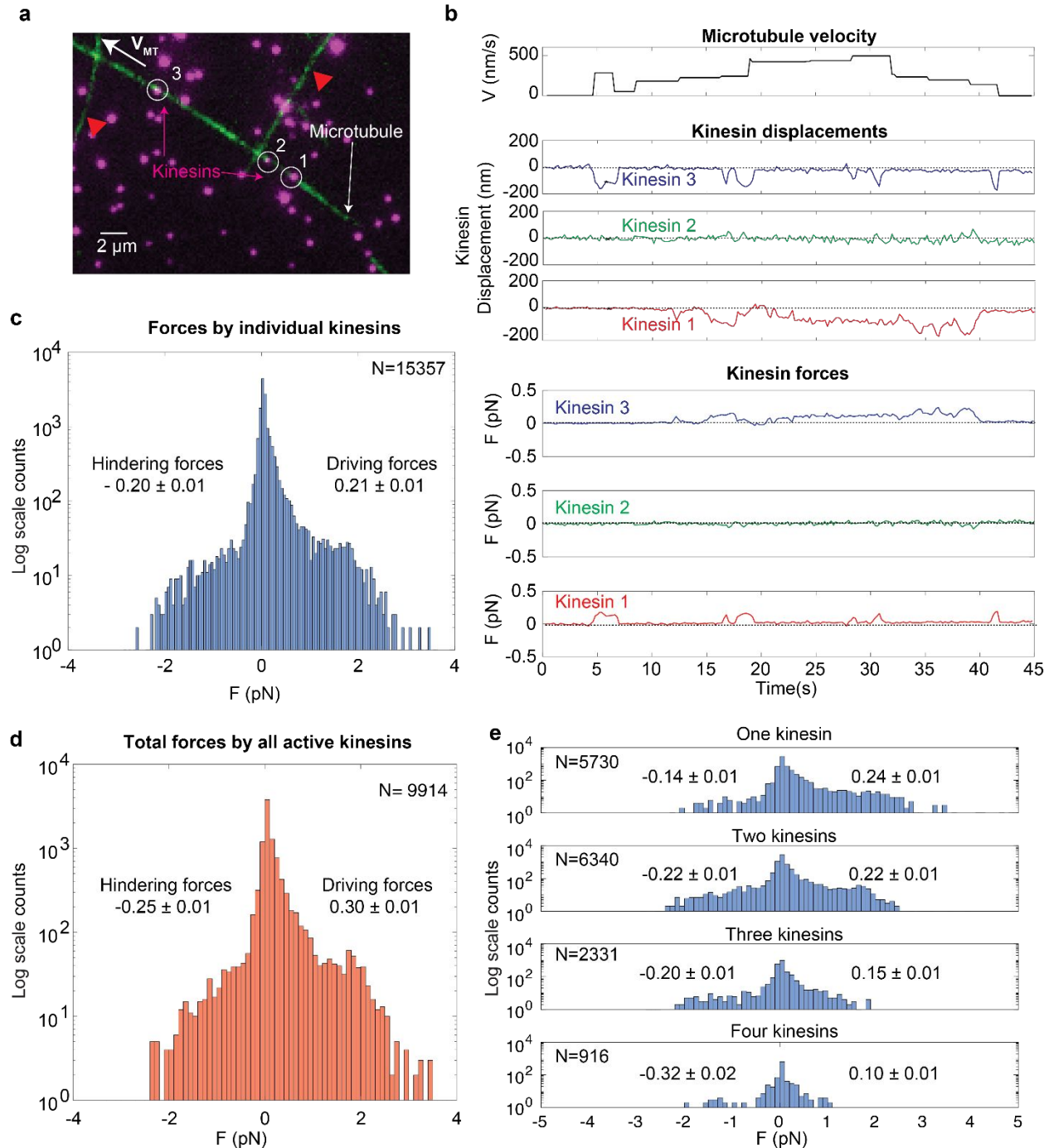


Figure 3 | Forces by individual kinesin motors. (a) Force dynamics of individual kinesin motors in a case where three kinesins (magenta, enclosed with white circles) are simultaneously transporting a common microtubule (green). The white arrow (V_{MT}) shows the direction of microtubule velocity. Red triangles indicate two other microtubules that interact with the microtubule transported by three kinesins. (b) Microtubule velocity, kinesin displacements, and individual forces of kinesins. (c) Histogram of force produced by individual kinesin motors during cargo transport. Forces are recorded when a kinesin is transporting a microtubule. This was determined when a kinesin was observed to be directly below a gliding microtubule in the microscope movie. Kinesins produce an average of 0.21 ± 0.01 pN force in the forward direction and 0.20 ± 0.01 pN of force in the backward direction (mean \pm s.e.m.). (d) Total force by all the kinesins that are actively exerting force at a particular time point on the microtubule is plotted. The average

total force on the microtubule is 0.30 ± 0.01 pN in the forward and 0.25 ± 0.01 pN in the backward direction. (e) Average forces exerted by individual kinesin motors with varying number of total kinesins. The average forward force per kinesin decreases as the number of kinesins increases. The average backward force increases as the number of kinesins increases.

Forces by individual kinesin motors during multi-motor transport

An example of a microtubule (green) transported by three kinesin motors (magenta, enclosed in white circles) is shown in Fig. 3a. As soon as the microtubule became attached to the kinesins, the kinesins began walking on the microtubule and were moved from their equilibrium positions. We determined that a kinesin was bound to a microtubule if it was observed directly below a gliding microtubule in the microscope movie. We plotted the microtubule velocity (Fig. 3b top panel) and the displacements of each of the three kinesins with time (Fig. 3b middle panels). Using kinesin displacements and reference force-extension curve, we estimated the force exerted by each kinesin on the microtubule during collective transport (Fig. 3b bottom panels). We observed that individual kinesins' forces varied dynamically with time. For example, kinesin #1 and #3 applied positive forces intermittently, while kinesin #2 remained at its equilibrium position under the microtubule for the entire transport duration and exerted negligible forces.

To make sense of the forces generated by individual kinesins, we carried out a control, measuring the forces with kinesins at their equilibrium position (Fig. S6). When there is no microtubule attached to kinesins, kinesins remain at their equilibrium position, and the forces generated are close to zero. We also observed microtubules transported by a single kinesin (Fig. S7). Forces by one attached kinesin remain very low. In fact, this makes sense: For transporting a microtubule, one kinesin needs to produce a force comparable to the drag force on the microtubule, which is expected to be < 0.1 pN (see supplementary text S3)^[31]. As per the newton's law, forces by the kinesins and drag force on the microtubule should add up to zero. In the case of Fig. 3a, the microtubule moved by three kinesins interacted with two other microtubules (red triangles), which prompted the kinesins to increase their forces for the continuation of the transport, as shown in Supplementary Movie 2. At other times, e.g., from $t = 7$ to 12 s, the microtubule is moving with no appreciable load, i.e., the forces exerted by kinesins are undetectably small.

To delve into the statistics of force exerted by kinesin motors during collective transport, we analyzed 82 instances (82 independent microtubules) where a microtubule was being transported by multiple kinesins and obtained thousands of kinesin force data points ($N = 15357$, N represents the number of the force data points with the frame rate of 0.2 s; see also Fig. S8-9 for discussion of other cases). We plotted the histograms of forces produced by individual kinesin motors (Fig. 3c). Kinesins exerted forces in the forward direction most of the time—76% of the force data points were in the direction of microtubule velocity—and 24% of forces were in the negative direction and hindered the transport of the microtubule. This observation is consistent with our previous study where we had observed that 70% kinesins remained in driving state[6]. Kinesins exerted an average of 0.21 ± 0.01 pN force during the collective transport of microtubules in the positive direction and an average of 0.20 ± 0.01 pN of force in the negative direction (Fig. 3c). Our

experimental force values agree with previously determined theoretical predictions^[32]. With our assay, it is not possible to visualize molecular interactions of kinesins with the microtubule. Therefore, there could be some kinesins with low displacement that are unbound to the microtubule. To determine the upper limit of the average kinesin forces, we eliminated the kinesin forces that had less than 20 nm displacement and recalculated the average forces (Fig. S22). Average force of driving and hindering kinesins in this case is 0.254 ± 0.004 pN and -0.27 ± 0.01 pN, which is slightly higher than the reported force in Fig. 3c. We also calculated the total forces on the microtubule by adding the forces of all the kinesins that either drove (+) or hindered (-) the microtubule motion at a given point of time. The average total force exerted by the kinesins was 0.30 ± 0.01 pN in the forward direction and was marginally higher than the average individual kinesin force of 0.21 ± 0.01 pN (Fig. 3d). Although individual kinesins exert more than 1 pN forces occasionally (see Fig. S10), each needs to produce much smaller forces on average for transporting the cargo than its stall force of 5-7 pN^[33-35].

Our assay also allowed us to quantify the effect of the number of kinesins on individual kinesin forces. We segregated the cases by quantifying the exact number of kinesins transporting a microtubule at a given point of time. As the total number of kinesins increases on the microtubule, the average force per kinesin in the positive direction decreases, indicating that driving kinesins share the load amongst themselves during the collective cargo transport (Fig. 3e). Interestingly, the average negative force by kinesins increases with the increasing number. As discussed earlier, the number of driving kinesins is almost three-times that of hindering kinesins. As the total number of kinesins on the cargo increases, the hindering kinesins must balance the forces by a higher number of driving kinesins, and therefore need to exert higher forces.

Kinesin forces in the presence of artificial roadblocks

In cells, molecular motors need to overcome many roadblocks to reach their destination. To mimic cellular roadblocks, we attached fluorescent quantum dots (QD605, 25-20 nm in size) to the microtubules using streptavidin-biotin linkages and used these QD-decorated microtubules in our force sensor assay. After roadblock QDs were attached to the microtubules, we saturated all the streptavidins on the roadblock QDs with excess biotin to avoid unintended streptavidin-biotin interactions. We could track the dynamics of kinesins, roadblocks, and microtubule simultaneously using a three-camera experimental setup (Fig. 1b).

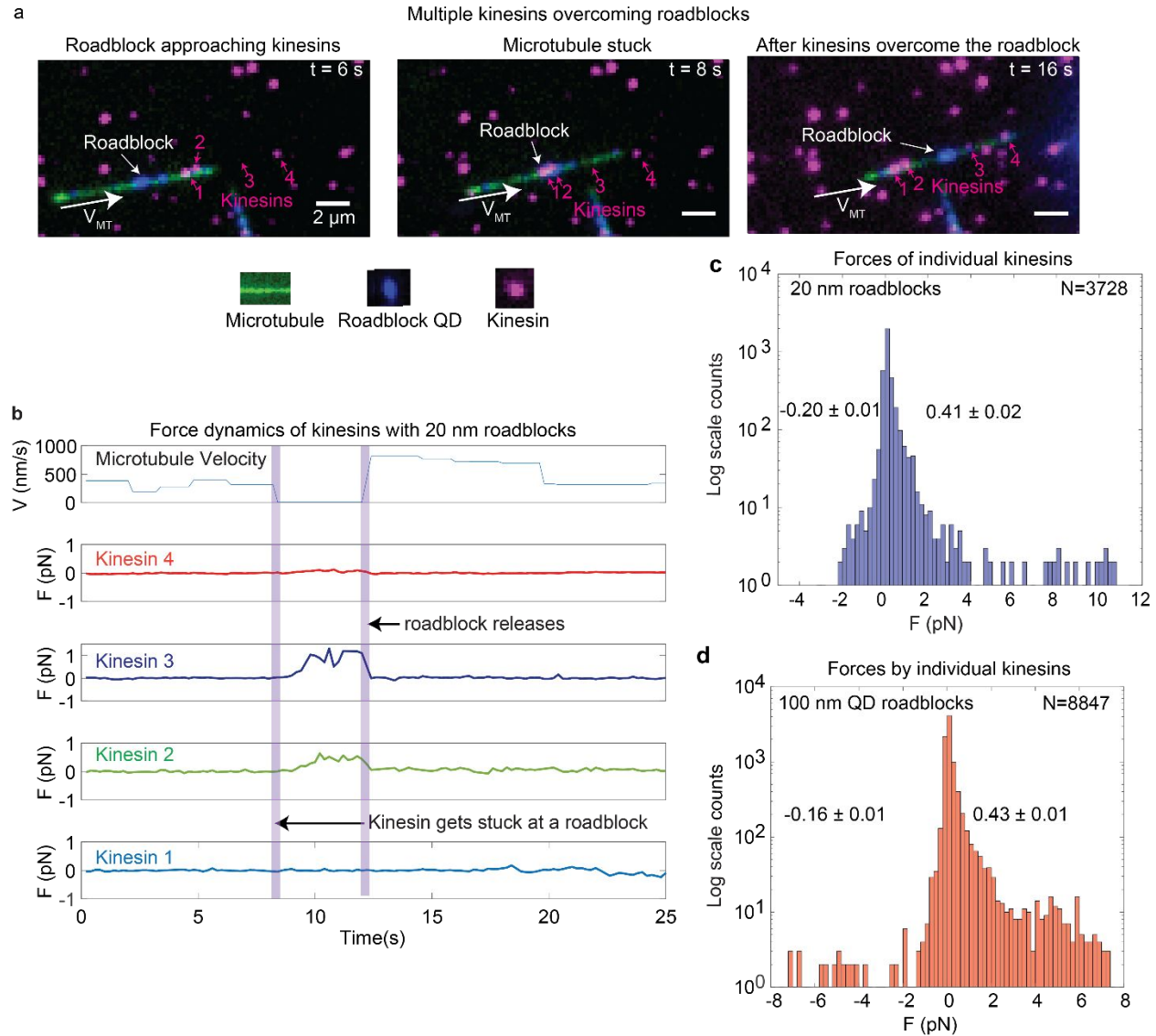


Figure 4 | Force dynamics of kinesins in the presence of 20-nm quantum dots as roadblocks. (a) Microscope images of an instance at different time points where four kinesins overcome a roadblock. Microtubule, kinesins, and roadblocks are shown in green, magenta, and blue colors, respectively. The white arrow shows the microtubule velocity direction. One of the kinesins (kinesin #1) becomes stuck on the roadblock on the microtubule at $t = 8$ s (middle image). The rightmost image illustrates when kinesins have overcome the roadblock, and the microtubule starts moving again. The fluorescence intensity of kinesin #3 is dim in the first two images as it is out of focus. **(b)** Forces by four kinesins are plotted when they are simultaneously moving a common microtubule. Microtubule velocity is also plotted. The vertical purple rectangles depict the time points when one kinesin becomes stuck at the roadblock ($t = 8$ s) and when the roadblock is released ($t = 13$ s). Microtubule transport resumes after kinesin #2 and #3 apply forces between $t = 8$ s and $t = 13$ s. **(c)** Force histogram of kinesins in the presence of roadblocks. Kinesins exert 0.41 ± 0.02 pN and 0.20 ± 0.01 pN force on an average in the forward and backward direction, respectively, in the presence of the roadblocks (mean \pm s.e.m.). **(d)** We record the forces exerted by kinesins transporting the roadblock (100 nm QDs) loaded microtubules (38 independent microtubules). In the presence of 100 nm roadblocks, the mean forces of kinesins remain 0.43 ± 0.01 pN and 0.16 ± 0.01 pN in the forward and backward direction, respectively (mean \pm s.e.m.).

To quantify the forces exerted by kinesins in the presence of the roadblocks, we analyzed the movement of kinesins and QD-decorated microtubules. We observed that as roadblocks were introduced in the system, the motion of the microtubule became less smooth, and there were more occurrences of stopping and bending of microtubules. We illustrate one of the cases where four kinesins transport a microtubule in Fig. 4a. Initially, the microtubule attached to kinesins and started moving, and we observe the microtubule and the roadblocks approaching the kinesins (Fig. 4a left, $t = 6$ s). We plotted the forces exerted by each kinesin and the microtubule velocity with time (Fig. 4b). One of the kinesins (kinesin #1) became stuck at the roadblock at $t = 8$ s (Fig. 4a middle, vertical purple rectangle in Fig. 4b). At this point, kinesin #2 and #3 exerted higher forces, and kinesin #1 did not increase its force and remained stuck. The stuck kinesin bypassed the roadblock, and the microtubule started moving again at time $t = 12$ s (Fig. 4a right; snapshot shown at $t = 16$ s). After bypassing the roadblock, the forces of all the kinesins decreased as the kinesins needed to apply only low forces, those comparable to the drag forces on the microtubule. The cartoon of the positions of the kinesins and the roadblock is shown in Fig. S21. Forces of the three kinesins remained much below the stall force even when a kinesin became stuck at the roadblock. This instance demonstrates that multiple kinesins can simultaneously increase their forces marginally, overcoming the roadblocks (See supplementary movie 3). We discuss more cases where kinesins dynamically change their force in the presence of roadblocks in the supplementary information (Fig. S11-13).

We analyzed 40 instances (40 independent microtubules) of the roadblock-loaded microtubule transport by multiple kinesins to obtain the aggregate force characteristics (Fig. 4c). We found that the average force exerted by kinesin motors marginally increases when the quantum dot roadblocks are introduced in the assay. In addition, with roadblocks, kinesin occasionally reached forces comparable to its stall force (1.4% force data points were >5 pN) but primarily remained in the sub-pN regime (Fig. 4c). Kinesins produced an average of 0.41 ± 0.02 pN in the positive direction and 0.20 ± 0.01 pN in the negative direction, with QD605 as roadblocks. Next, we asked if the force exerted by kinesin increases if we increase the size of the roadblocks. Therefore, we used 100-nm microspheres (compared to the 20 nm QD) as roadblocks. These microspheres had streptavidin conjugated on their surface, which facilitated attachment to biotinylated microtubules. We analyzed 38 such cases and plotted the force histogram (Fig. 4d). Kinesins exerted an average force (per kinesin) of 0.43 ± 0.01 pN in the forward direction and 0.16 ± 0.01 pN in the backward direction, which is comparable to the forces in the presence of QD605 as roadblocks (Fig. 4c). These results show that kinesins primarily exert less than 1 pN forces even in the presence of the roadblocks and rarely (Figure S10 and S14), but occasionally, increase their forces to their stall forces.

Conclusion

In this work, we have leveraged the power of fluorescence microscopy to develop a ssDNA_{DEN}-based Force Sensing of Individual Motors (FSIM) assay. Our assay can visualize individual motors and measure their forces during multi-motor transport of a common microtubule cargo. We performed optical trap assay measurements to characterize the force-extension properties of the

ssDNA_{DEN} molecule that acts as a force sensing molecule in the FSIM assay. Our FSIM assay adds high-throughput and single-motor resolution method to the repertoire of available force spectrometry techniques. The in-house developed MiCA purification minimized the presence of unlabeled kinesins in our assay.

Our technique, naturally, also has some limitations. For example, other effects on the force measurements are possible, such as unlabeled kinesins, microtubule defects, the interaction of microtubules with the surface, etc., that are not observed with our assay. We believe the investigation of these effects will be possible with future studies involving techniques like atomic force microscopy, where the defects on the microtubule lattice can be observed. Fluorescence microscopy-based techniques, are, in general, not used for studying microtubule lattice defects. Another limitation of our technique is the inability to conclusively assess whether a motor is bound to the microtubule. However, this limitation does not introduce errors in force calculation as unbound motors exert zero forces and our assay is able to measure these zero forces. For the motors that are bound and are in either driving or hindering positions, our assay measures forces accurately.

Another possible problem is that there may be kinesins in our assay that have multiple ssDNA_{DEN} tethers and follow the characteristics of this secondary cluster (which is also seen in the optical trap assay, Fig. S5). To test for this, we used 5x excess of kinesin-QD with ssDNA_{DEN} and, therefore, approximately 2% of kinesins would have multiple tethers in our assay. We have analyzed our data by assuming 2% of the kinesins follow secondary cluster force-extension behavior and provided the force statistics in Fig. S19. We conclude that forces remain comparable to the reported forces in Fig. 3, even when we take the secondary cluster effects into account. We also note that the microtubule velocities are lower when a ssDNA_{DEN} tethers are present in the assay in comparison to when dsDNA tethers are used (as shown in our previous publication Tjioe et al., eLife, 2019). However, kinesin duration on the microtubule does not change when the tethers are replaced from dsDNA to ssDNA_{DEN} (Fig. S20). Therefore, we have some evidence to suggest that the type of the tethering molecule affects the molecular mechanism of multiple kinesin based cargo transport.

In summary, the use of denatured single-stranded DNA in this study enables the measurement of individual kinesin forces that was not possible with the use of dsDNA. Our assay is versatile and can be used to study the force dynamics of motors in diverse configurations, such as the presence of a variety of roadblocks. We have shown that kinesins keep their forces primarily below one pN and can still overcome the roadblocks by modulating their forces. Kinesins have been shown to produce up to 7 pN force using optical trap assays which is the maximum force that a kinesin can produce when an opposing force is applied. Our results do not contradict these previous measurements for measuring the maximum force: rather, what we show is that in our assays when kinesins work in teams in our assays, the maximum force is rarely reached and individual kinesins produce 1 pN force on an average during multi-motor transport. We have also shown that driving kinesins share the load amongst themselves during multi-motor transport as individual motor

forces decrease when the number of motors increases on the cargo. We surmise that multiple motors help to maintain directed motion: at times, a kinesin comes off while others maintain the direction of the cargo. In general, we believe our work is the most direct measurement of individual motors and their forces while they transport the cargo in teams. Our assay provides a basis for future studies involving more complex force-sensing assays that mimic cellular environments closely. Furthermore, our FSIM assay is expected to be useful for understanding the motion of opposite-directed and different motors.

Methods

Kinesin purification:

Truncated kinesin with 888 amino acids (K888) from the mouse kinesin heavy chain (accession number BC090841) with a C-terminal biotin-tag and FLAG epitope, and mouse kinesin light chain (accession number BC014845) were cloned separately into the baculovirus transfer vector pAcSG2 (BD Biosciences) for recombinant virus production. The C-terminal biotin tag was added for the attachment of kinesin to microscope coverslips or streptavidin labeled quantum dots. This biotin tag was an 88 amino acid long sequence from *Escherichia coli* biotin carboxyl carrier protein^[36] which was biotinylated at a single lysine during expression in Sf9 cells. A FLAG epitope followed the biotin tag at the C-terminal facilitated purification by affinity chromatography. This constitutively active truncated kinesin (K888) with bound light chain was purified as described previously^[6]. SDS-PAGE gel image of a representative protein preparation is shown in Fig. S15. Briefly, Sf9 cells were infected with Baculovirus. The growth medium was supplemented with 0.2 mg/ml biotin. Cells were harvested after 72 hours and were lysed by sonication in 10 mM imidazole, pH 7.4, 0.3 M NaCl, 1 mM EGTA, 5 mM MgCl₂, 7% (w/v) sucrose, 2 mM DTT, 0.5 mM 4-(2-aminoethyl) benzenesulfonyl fluoride, 5 µg/ml leupeptin. Lysed cells were clarified at 200,000 g for 40 min. The supernatant was collected and was purified using FLAG-affinity chromatography (Sigma-Aldrich). The column was washed with the washing buffer (washing buffer contained 10 mM imidazole, 0.3 M NaCl, and 1 mM EGTA, pH 7.4). Protein was eluted using the washing buffer supplemented with 0.1 mg/ml FLAG peptide. The protein fractions were concentrated with Amicon centrifugal filter device (Millipore). The protein was dialyzed against 10 mM imidazole, pH 7.4, 0.2 M NaCl, 1 mM tris(2- carboxyethyl)phosphine TCEP), 55% (v/v) glycerol, 1 mM DTT, 1 µg/ml leupeptin and 50 µM MgATP for storage at -80°C.

Magnetic cytoskeleton affinity (MiCA) purification of quantum dot-labeled kinesin

Kinesin conjugated with quantum dots (Kinesin-QD) was purified from the free QDs using the in-house developed MiCA purification^[26]. Kinesin was mixed with 3x more quantum dots (QD705 streptavidin conjugate, Catalog Number: Q10163MP, ThermoFisher). Kinesins bound to QDs with biotin-streptavidin linkage as kinesin had a biotin modification and every QD had multiple streptavidins present on its surface. BSA supplemented DMB buffer (dynein motility buffer: 30 mM HEPES, 50 mM KAcetate, 2 mM MgAcetate, 1 mM EGTA, pH 7.2 with 8 mg/ml BSA) was used for dilutions of kinesin and quantum dots. The mixture of kinesin and quantum dots was incubated for 10 minutes at room temperature. Short GMPCPP microtubules were prepared by incubating the 1 mg/mL 97% pure tubulin (HTS03-A, Cytoskeleton, Inc.) with 2.3 mM GMPCPP at 37° C followed by sonication for 3 minutes. GMPCPP microtubules were aliquoted in small tubes and stored at -80° C for long term storage. For every MiCA purification experiment, aliquots of GMPCPP-microtubules were as thawed. In a separate tube, moderately positive charged magnetic beads (i.e., magnetic amine beads coated with PEG-amine to reduce highly positive amine charge) were mixed with short GMPCPP-microtubules. Magnetic beads and GMPCPP microtubules were incubated for 5 minutes to facilitate their assembly. Magnetic beads were placed in the magnet and the supernatant was discarded. The pellet containing magnetic beads and GMPCPP microtubules was washed with 8 µL of DMB-BSA-Taxol buffer (DMB-BSA buffer containing 20 µM paclitaxel). Magnetic force was applied again to make the pellet and the pellet was

reconstituted in 1 μL of DMB-BSA-Taxol buffer. Next, 6 μL of kinesin-quantum dot was mixed with the reconstituted mixture of magnetic bead-GMPCPP microtubules in the presence of 1 mM AMPPNP and incubated for 5 minutes at room temperature in an end-to-end rotator. AMPPNP caused kinesins to bind strongly to the GMPCPP microtubules. The mixture was washed 3x with DMB-BSA-Taxol buffer to remove excess quantum dots from the mixture while kinesin-QD remained bound to the pellet. Kinesin-QD were eluted with 8 μL of elution buffer in end-to-end rotor by incubating for 5 minutes at room temperature. The eluant was collected that contained purified kinesin-QD (80 nM kinesin-QD, assuming 50% purification yield).

Microtubule preparation and polymerization:

Tubulin, biotin-tubulin and Hylite-488-tubulin (all tubulin proteins were purchased from Cytoskeleton Inc.) were mixed together in 16:2:1 (w/w) ratio. This mixture was stored in small aliquots in -80°C . The tubulin mixture was polymerized at 37°C for 30 minutes in the presence of 10% (v/v) glycerol and 2 mM GTP. Polymerized microtubules were centrifuged at 13000g for 30 minutes at room temperature. Supernatant was discarded and the pellet of polymerized microtubules was reconstituted in the buffer containing 1 mM GTP (Cytoskeleton Inc.) and 200 μM paclitaxel (Cytoskeleton Inc.).

Synthesis of glyoxal denatured single-stranded DNA (ssDNA_{DEN}):

The length of ssDNA_{DEN} (1180 bp with 500 nm contour length) was chosen such that each kinesin could move sufficiently around its equilibrium position without interfering with other kinesins. The process of ssDNA_{DEN} synthesis is shown in Fig. 2a. pBR322 plasmid (NEB, catalog #N3033S) was used as a vector for PCR amplification of 1116 bp long dsDNA using primers P1 and P2 (sequences of all primers are given in Table S1). Primer P1 had a digoxigenin modification at its 5' end. All primers were ordered from IDT. The PCR product was digested with PspGI restriction enzyme (NEB, catalog #R0611S) to obtain a 1080 bp long DNA with 5 bp overhang and was subsequently dephosphorylated with Antarctic phosphatase (NEB, catalog #M0289S). The obtained product was PCR purified using a Qiagen PCR purification kit, and the concentration was measured using Nanodrop One (ThermoFisher). The obtained DNA product (1080 bp) was annealed with primer P3 (100 bp long) at a 1:3 DNA to primer molar ratio and ligated using T4 DNA ligase (NEB, catalog #M0202S). Primer P3 had a biotin modification at its 3' end. After the ligation, we obtained a dsDNA product that had one strand functionalized with digoxigenin at one end and biotin at the other end. The length of this molecule was 1180 bp.

Next, we denatured the DNA with glyoxal^[25] to obtain the final denatured single-stranded DNA, ssDNA_{DEN}. First, glyoxal was deionized using a mixed bed resin (AG 501-X8, BioRad, Hercules, CA, USA). 10 ml of glyoxal was treated with 2 g of mixed bed resin and was stirred for 2 hours. The deionization process was repeated three times.

Glyoxal treatment of 1180 bp long dsDNA was carried out in TE buffer (ThermoFisher) with a reaction volume of 20 μL . Reaction volume contained 50% v/v DMSO and 1 M glyoxal. Glyoxal treatment was carried out at 50°C for 1 hour in a PCR thermocycler (Eppendorf). The final product was run on 1% agarose gel in TBE buffer for 1 hour at 100V. ssDNA_{DEN} on the gel was stained with SYBR gold stain and was gel purified with a QIAquick gel extraction kit (Qiagen) (Fig. S16). The concentration of ssDNA_{DEN} was measured with NanoDrop One (ThermoFisher).

Treatment of ssDNA with glyoxal eliminated secondary structure formation of single-stranded DNA. Secondary structures introduce conformational variability amongst ssDNA molecules that translate to inconsistent force measurement.

Optical Trapping Assay

The stretching behavior of glyoxalated single-stranded DNA (ssDNA_{DEN}) in the same buffer conditions as the microtubule assay was characterized by pulling on individual molecules using dual-trap optical tweezers^[28,29].

Glyoxalated single-stranded DNA molecules identical to those used in the microtubule assay (i.e., 1180-nt long, functionalized with 3' biotin and 5' digoxigenin) were synthesized as described earlier above. For optical trapping experiments, ssDNA_{DEN} was diluted to 0.14 nM, and 1 to 1.5 μ L of the ssDNA_{DEN} solution was incubated for an hour at room temperature with 5 μ L of 0.2% w/v streptavidin-coated microspheres (Spherotech). Beads were diluted in approximately 300 μ L of buffer (100 mM Tris, 20 mM NaCl, 3 mM MgCl₂, pH 7.6) for delivery to the optical traps through bead channels in a custom flow chamber^[37].

The trapping channel of the flow chamber contained buffer consisting of: 91% DmB-BSA (30 mM HEPES, 5 mM MgSO₄, 1 mM EGTA, 8 mg/ml BSA, pH 7.0), 10 μ M biotin, 100 μ M ATP, 100 μ M THP, 2 μ M Paclitaxel, and an oxygen scavenging system^[38,39] (final concentrations in buffer: 8 mg/mL glucose, 0.15 mg/mL catalase (from *Aspergillus niger*: Millipore Sigma, formerly EMD Millipore, 219261-100KU, 5100 U/mg), 0.29 mg/mL pyranose oxidase (from *Coriolus sp.*: Sigma P4234-250UN, 12.2 U/mg), 100 μ M Tris-HCl and 100 μ M NaCl). In this trapping channel, dual-trap optical tweezers were used to trap a ssDNA_{DEN}-coated streptavidin microsphere in one trap, and a microsphere (Spherotech) coated with anti-digoxigenin antibody (Roche Diagnostics) in the other. The microspheres were repeatedly brought together until a ssDNA_{DEN} tether formed between them.

Once a ssDNA_{DEN} tether formed between the two trapped microspheres, force-extension curves (FECs) were collected by moving one trap away from the other at a constant rate (10 nm/s or 100 nm/s) over a pre-set distance, then returning at the same rate to the initial position. Multiple force extension curves were collected per tether, preferably until the tether ruptured, allowing us to observe the variability of the behavior of a single molecule. A single, one-step rupture of the tether was taken as a strong indication that the tether had consisted of a single molecule. At the low ssDNA_{DEN} concentrations used, only a small fraction of bead pairs (approximately 10%) formed tethers, decreasing the probability of multiple tethers forming.

Optical Trapping Data Processing

Before the force extension curves could be used for calibration of ssDNA_{DEN} as a force sensor, the extension measured in optical trapping experiments was offset-corrected. The measured extension differs slightly from the absolute end-to-end extension of the molecule, owing to the difference in nominal and actual microsphere diameter and an instrumental offset. For measurements of a molecule with well-characterized stretching behavior, this offset is determined and corrected through fitting its force extension curve to the appropriate theoretical model, with the extension offset as the single fitting parameter. In the absence of such a model for ssDNA_{DEN}, we determined the offset (under the same conditions) by fitting the force extension curve of a well-characterized DNA hairpin construct to the extensible worm-like chain model^[40,41]. The average offset was determined to be 60 nm. Variations in microsphere diameter were small: the standard deviation of the extension offset was 5 nm for the control construct, and the control set of force extension curves spanned 25 nm at 15 pN. All reported ssDNA_{DEN} extensions were offset-corrected by 60 nm.

Out of 72 collected force extension curves, 64 formed a cluster with similar curvature (Fig. S5). We interpreted this 'primary cluster' as representing the typical behavior of ssDNA_{DEN}. The vast majority of these, 58 force extension curves, had no significant rips or discontinuities; this set was used to determine a calibration force-extension curve for ssDNA_{DEN} for the kinesin experiments. First, a single 'net' force extension curve for each bead pair was obtained from a weighted average of all force extension curves, binned in force, from that bead pair. The resulting six net force extension curves were fitted to a model based on previously published data and models of ssDNA_{DEN} behavior^[27,30]. These published data show that the extension L of ssDNA_{DEN} under force F follows a power law, $L \sim F^\gamma$ with $\gamma \approx 2/3$ at low forces, in solutions containing either monovalent or divalent ions^[27,30]. At higher forces, L varies logarithmically with force in solutions containing monovalent ions only. Inspection of the rescaled force extension curves in solutions containing divalent ions (Fig. 3 of Ref.^[30]) suggests that the extension may follow a power law with a different exponent over at least part of the higher force range. We therefore fitted our optical trapping data to the following expression:

$$L = d \cdot \left(\frac{F}{F_0} \right)^{\gamma(F)}$$

where F_0 is a constant equal to 1 pN, and in which the force-dependent exponent γ transitions between two values: the experimentally determined value 0.62 at low force^[30], and the value $0.62 - a$ at high force:

$$\gamma(F) = \frac{a}{(1 + e \cdot F)} + 0.62 - a$$

The force extension curves of ssDNA_{DEN} were fit to this expression with a , d , and e as fitting parameters. The resulting coefficients, with standard errors, are: $a = 0.365 \pm 0.003$, $d = 273 \pm 2$ nm, and $e = 5.6 \pm 1.5$ pN⁻¹.

Fitting was carried out on six averaged force extension curves, one per bead pair—rather than directly on the set of 58 force extension curves—to avoid biasing the fits through properties of beads that yielded more force extension curves. Factors specific to each bead pair, in particular any deviation of the beads' diameters from the average values, and the resulting errors in calibration of the optical trap stiffness, affect all force extension curves from that bead pair in the same manner; these force extension curves cannot therefore strictly be treated as independent. Instead, each force extension curve from a given bead pair was binned by force; the mean extension and standard error of the mean extension in each bin was used to calculate a weighted average of extension from all force extension curves from the bead pair for that bin. The resulting extension per force bin comprised the net force extension curve for the bead (Fig. 2c, colored symbols; different colors denote net force-extension curves from different bead pairs, and uncertainties of weighted averages are smaller than marker size). The resulting six net force extension curves were then fitted with the model with an unweighted fit. Force-extension data below 0.2 pN were not included in the fit: at those forces, the molecular extension for this construct is sufficiently low that the measurements become inaccurate due to artefacts, in particular cross-talk between the two optical traps. Our obtained analytical model was used as a reference curve to calculate the forces from displacements.

Stretching behavior of ssDNA_{DEN}: variability and clustering

Figure S5 shows all force extension curves collected, color-coded by bead pair (10 in total). While tethers from a given bead pair may be different molecules, some may be previously measured molecules re-tethered. Out of the 72 collected force extension curves of ssDNA_{DEN}, 64 fell into a 'primary' cluster, which we interpreted as the typical stretching behavior of the molecule.

The primary cluster exhibits considerable variation, resulting in a range of extensions at any given force. Some of this variability may arise from differences in microsphere diameter and from the resulting errors in calibration of the optical trap stiffness. However, we see appreciable variability in force extension curves taken from the same bead pair—pointing to heterogeneity in ssDNA_{DEN} molecules—and sometimes even from the same molecule pulled through multiple cycles. The variability in force extension curves can be considerable, spanning up to 40 or 50 nm in extension at 15 pN. We see no evidence of significant secondary structure formation, which could account for the variability. Variability in molecular stretching behavior of ssDNA_{DEN} has been observed previously. McIntosh and Saleh report variations in contour length from molecule to molecule and also between force extension curves of the same molecule, especially at high salt concentrations^[30]. These variations were attributed to non-specific adsorption to surfaces, but it is unclear if this would be relevant in our optical trap setup.

The remaining 10% of force-extension curves fall into a 'secondary' cluster, with a higher stiffness than those in the primary cluster, and were excluded from the analysis. The nature of the secondary cluster is uncertain. Although very low concentrations of ssDNA_{DEN} were used to maximize the probability of stretching unique molecules, we speculate that many of the force-extension curves in the secondary cluster arise from stretching of more than one molecule. The formation of multiple tethers in parallel or interactions between a single tethered ssDNA_{DEN} molecule and others extending from the DNA bead could lead to force being shared between two or more molecules and a higher stiffness.

Of the 8 force-extension curves in the secondary cluster, two follow closely the predicted curve for a double tether as calculated from the analytical model for a single ssDNA_{DEN} molecule (Fig. S5, black dotted line). Two other curves display a rupture onto the primary cluster, indicating that several molecules are stretched in parallel and that all but one eventually detach, leaving a single ssDNA_{DEN} tether. The remaining 4 force-extension curves show overlap with the above curves, pointing to the same type of interference by other ssDNA_{DEN} molecules. We also fit the set of 8 force-extension curves forming the secondary cluster, excluding portions that ruptured onto the first cluster, using the analytical model used to fit the first cluster (Fig. S5, black dash-dot line). A numerically stable fit was obtained with a simplified variant of the analytical expression with $\gamma = 0.62 - a$, and coefficients $a = 0.358$ and $d = 218$ nm. The secondary cluster fit is similar to the predicted double-tether force-extension curve, consistent with our claim that most force-extension curves in the secondary cluster correspond to multiple molecules stretched in parallel. Nevertheless, we cannot rule out alternate explanations. Some secondary force-extension curves could arise from rare intra- or inter-molecular cross-linking events during synthesis^[30,42], or from the variability in contour length described above.

Force sensor assay:

MiCA purified Kin-QD was mixed with ssDNA_{DEN} in 5x molar excess to maximize the probability of attachment of one ssDNA_{DEN} molecule per kin-QD molecule (kin-QD-ssDNA_{DEN}). The biotin end of ssDNA_{DEN} got attached to kin-QD, and the digoxigenin end remained free. Kin-QD-ssDNA_{DEN} was mixed with 1 mM biotin to saturate all streptavidin on the surface of the QD.

Twenty-two square-mm coverslips were covalently functionalized with PEG and 1% PEG-Biotin^[43]. Flow chambers were made by sandwiching double-sided tape between cleaned glass slides and PEG-functionalized coverslips. 600 nM streptavidin (Cat. No: 43-4302 from Thermo Scientific) was flowed in the flow chamber followed by washing with DMB-BSA (DMB buffer: 30 mM HEPES, 5 mM MgSO₄, 1 mM EGTA, 8 mg/ml BSA, pH 7.0). 10 nM of anti-digoxigenin-biotin was flowed in the chamber and washed after 5 minutes with DMB-BSA-biotin buffer (DMB-BSA buffer supplemented with 0.5 mM biotin). Presence of high concentration of biotin in the DMB-BSA-biotin buffer saturated all the streptavidins on the coverslip surface which minimized the binding of biotinylated microtubule or kinesin on the surface. Then, Kin-QD-ssDNA_{DEN} was flowed in the chamber so that the assembly attaches the surface with the linkage of digoxigenin on ssDNA_{DEN} and anti-digoxigenin on the surface. Kin-QD-ssDNA_{DEN} solution was diluted sufficiently such that kinesins on the coverslips can be tracked individually and do not fall within the diffraction limit distance. After the attachment of kin-QD-ssDNA_{DEN} on the surface, all the streptavidins on the surface and on the quantum dot were saturated by flowing 1 mM biotin in the flow chamber. Next, imaging buffer containing microtubules, 2 mM ATP, and deoxygenating agents (pyranose oxidase+glucose) was flowed into the chamber (final concentrations in buffer: 8 mg/mL glucose, 0.15 mg/mL catalase (from *Aspergillus niger*: Millipore Sigma, formerly EMD Millipore, 219261-100KU, 5100 U/mg), 0.29 mg/mL pyranose oxidase (from *Coriolus sp.*: Sigma P4234-250UN, 12.2 U/mg). Since all streptavidin molecules in the chamber were already saturated with biotin, microtubules did not stick to the surface and were glided by the kinesins. The flow chamber was immediately imaged after flowing of the imaging buffer. 1 μ l of 50 nM of QD605 streptavidin conjugate (Catalog Number: Q10103MP, ThermoFisher) was mixed with 1 μ l of biotinylated microtubules (6 μ M of microtubules) for mimicking the roadblocks, which corresponded to 1.6 QDs per micron length of the microtubule. The QD605-microtubule mixture was incubated for 20 minutes. Streptavidin molecules on the surface of QD605 were saturated with 1 mM biotin. QD605 coated microtubules were used for making the imaging buffer. Force sensor assay was performed as described before with imaging buffer that contained roadblock incubated microtubules. For the experiments involving 100 nm roadblocks, we used 100 nm streptavidin-coated fluorescent polystyrene particles (Kisker Biotech, Germany). We mixed 3x diluted nanoparticles with 1 μ l of microtubules (6 μ M of microtubules) and incubated for 10 mins. Microtubule-particle assembly was saturated with 1 mM biotin and was used to make the imaging buffer. For each type of experiments, 5-8 movies (technical replicates) were taken, each with 0.2s exposure time and 2000 frames.

Fluorescence Imaging:

Kinesin was labeled with QD705, and microtubules were labeled with hilyte488 and were simultaneously imaged on two camera system in total internal refraction fluorescence (TIRF) mode. Experiments were performed on an inverted light microscope (Olympus IX71) with Andor EMCCD (iXon DU-897E) cameras. Images were acquired at 100x magnification with oil immersion objective (Olympus UPlanSApo, NA 1.40). The sample was excited by a 488 nm blue laser (Coherent OBIS), and excitation light was reflected with 495 nm long-pass dichroic (Chroma). MultiCam (Cairn Research, UK) was used to split the kinesin and microtubule excitation signals to capture on two different cameras. The excitation signal was passed through a 685 nm (T685lpxr-UF3, UltraFlat, Chroma) long-pass filter to split kinesin and microtubule signals. Additional filters were installed for kinesin (710/40, Brightline, Semrock) as well as microtubule (560/80, Brightline, Semrock) signals just before the camera captured the image. Two thousand frames per movie were acquired at 0.2 second exposure time and variable EM gain. EM gain was chosen to get the maximal signal output without saturating the camera on a case by case basis.

For doing the roadblock experiment, three cameras on MultiCam were used to image kinesin, roadblocks, and microtubules simultaneously. QD605 were attached to microtubules using streptavidin-biotin linkage that mimicked roadblocks. The excitation signal was split first with a 670 nm long-pass filter. Fluorescence corresponding to wavelengths >685 was captured on the kinesin camera. Excitation light with wavelengths <685 nm was further split using 570 nm long pass filter for roadblock and microtubule channel. Light entering the roadblock channel was cleaned with an additional 600/80 (Brightline, Semrock) filter.

Analysis of acquired movies:

At the start of the experiment, images of a nanohole were obtained from every channel of MultiCam (Cairn Research, UK) and a transformation file was obtained by registering the images with a MATLAB program as described previously^[26]. Movies obtained from different cameras were registered with each other using the obtained transformation file. Kinesin displacements were calculated using the TrackMate^[44] plugin of ImageJ^[45] and in-house MATLAB code, as described previously^[6]. Microtubule velocity was calculated by manually tracing the kymographs of the microtubule using in-house developed MATLAB program. Force applied by individual kinesin was calculated using the model described in Fig. 2c with a MATLAB code.

Data availability

Data is available in the main text or the supplementary information text and files. All Single-molecule imaging raw datasets are available from the corresponding author upon request.

Materials availability

Reagents described in this work will be made available upon request to the authors.

Code availability

The custom codes for the data analysis used in this study are available from the corresponding author upon request.

Competing interests

The authors declare no competing financial interests.

Acknowledgments

This work was supported by the NIH grants R01 GM132392 (to P.R.S.), GM120353 (to Y.R.C.), R35

GM136288 (to K.M.T.) and by the NSF Physics Frontiers Center (PFC) grant PHY-1430124 (“Center for the Physics of Living Cells”).

Author contributions

Conceptualization: S.S., Y.R.C., and P.R.S.; Single-molecule experiments: S.S., N.S., and B.K.M.; ssDNA_{DEN} synthesis: S.S.; Optical trap experiments and model fitting: A.T and Y.R.C.; Kinesin purification: C.S.B. and K.T.; MATLAB scripts: S.S. and M.T.; Data analysis: S.S., N.S., and B.K.M.; Writing: S.S., A.T. Y.R.C., and P.R.S.; supervision: Y.R.C. and P.R.S.

References:

- [1] M. Schliwa, G. Woehlke, *Nature* **2003**, *422*, 759.
- [2] J. Howard, *Nature* **1997**, *389*, 561.
- [3] A. Habermann, T. A. Schroer, G. Griffiths, J. K. Burkhardt, *J. Cell Sci.* **2001**, *114*, 229.
- [4] P. L. Leopold, A. W. McDowall, K. K. Pfister, G. S. Bloom, S. T. Brady, *Cell Motil. Cytoskeleton* **1992**, *23*, 19.
- [5] S. P. Gross, M. Vershinin, G. T. Shubeita, *Curr. Biol.* **2007**, *17*, 478.
- [6] M. Tjioe, S. Shukla, R. Vaidya, A. Troitskaia, C. Bookwalter, K. M. Trybus, Y. R. Chemla, P. R. Selvin, *Elife* **2019**, *8*, 1.
- [7] V. Siahaan, J. Krattenmacher, A. A. Hyman, S. Diez, A. Hernández-Vega, Z. Lansky, M. Braun, *Nat. Cell Biol.* **2019**, *21*, 1086.
- [8] A. R. Chaudhary, F. Berger, C. L. Berger, A. G. Hendricks, *Traffic* **2018**, *19*, 111.
- [9] K. Svoboda, S. M. Block, *Cell* **1994**, *77*, 773.
- [10] C. M. Coppin, D. W. Pierce, L. Hsu, R. D. Vale, *Proc. Natl. Acad. Sci.* **2002**, *94*, 8539.
- [11] A. Kunwar, M. Vershinin, J. Xu, S. P. Gross, *Curr. Biol.* **2008**, *18*, 1173.
- [12] B. H. Blehm, T. A. Schroer, K. M. Trybus, Y. R. Chemla, P. R. Selvin, *Proc. Natl. Acad. Sci.* **2013**, *110*, 3381.
- [13] A. K. Rai, A. Rai, A. J. Ramaiya, R. Jha, R. Mallik, *Cell* **2013**, *152*, 172.
- [14] S. C. Kuo, M. P. Sheetz, *Science* **1993**, *260*, 232.
- [15] K. Furuta, A. Furuta, Y. Y. Toyoshima, *Proc. Natl. Acad. Sci.* **2013**, *110*, 501.
- [16] A. T. Blanchard, K. Salaita, *Science* **2019**, *365*, 1080.
- [17] C. Albrecht, K. Blank, M. Lalic-Mülthaler, S. Hirler, T. Mai, I. Gilbert, S. Schiffmann, T. Bayer, H. Clausen-Schaumann, H. E. Gaub, *Science* **2003**, *301*, 367.
- [18] X. Wang, T. Ha, *Science* **2013**, *340*, 991.

- [19] J. M. Brockman, A. T. Blanchard, V. Pui-Yan, W. D. Derricotte, Y. Zhang, M. E. Fay, W. A. Lam, F. A. Evangelista, A. L. Mattheyses, K. Salaita, *Nat. Methods* **2018**, *15*, 115.
- [20] D. M. J. Lilley, T. Ha, *Science* **2007**, *1909*, 279.
- [21] J. J. Funke, P. Ketterer, C. Lieleg, S. Schunter, P. Korber, H. Dietz, *Sci. Adv.* **2016**, *2*, e1600974.
- [22] P. C. Nickels, B. Wunsch, P. Holzmeister, W. Bae, L. M. Kneer, D. Grohmann, P. Tinnefeld, T. Liedl, *Science* **2016**, *354*, 305.
- [23] M. Urbanska, A. Lüdecke, W. J. Walter, A. M. van Oijen, K. E. Duderstadt, S. Diez, *Small* **2021**, *2007388*, 1.
- [24] M. A programmable DNA origami nanospring that reveals force-induced adjacent binding of myosin VI heads Iwaki, S. F. Wickham, K. Ikezaki, T. Yanagida, W. M. Shih, *Nat. Commun.* **2016**, *7*, 1.
- [25] G. K. McMaster, G. G. Carmichael, G. Gordon, *Proc. Natl. Acad. Sci. U. S. A.* **1977**, *74*, 4835.
- [26] M. Tjioe, H. Ryoo, Y. Ishitsuka, P. Ge, C. Bookwalter, W. Huynh, R. J. McKenney, K. M. Trybus, P. R. Selvin, *Bioconjug. Chem.* **2018**, *29*, 2278.
- [27] O. A. Saleh, D. B. McIntosh, P. Pincus, N. Ribeck, *Phys. Rev. Lett.* **2009**, *102*, 1.
- [28] J. R. Moffitt, Y. R. Chemla, D. Izhaky, C. Bustamante, *Proc. Natl. Acad. Sci. U. S. A.* **2006**, *103*, 9006.
- [29] C. Bustamante, Y. R. Chemla, J. R. Moffitt, *Cold Spring Harb. Protoc.* **2009**, *4*, DOI 10.1101/pdb.ip73.
- [30] D. B. McIntosh, O. A. Saleh, *Macromolecules* **2011**, *44*, 2328.
- [31] A. J. Hunt, F. Gittes, J. Howard, *Biophys. J.* **1994**, *67*, 766.
- [32] H. Palacci, O. Idan, M. J. Armstrong, A. Agarwal, T. Nitta, H. Hess, *Langmuir* **2016**, *32*, 7943.
- [33] M. J. Schnitzer, K. Visscher, S. M. Block, *Nature* **1999**, *400*, 184.
- [34] M. Nishiyama, H. Higuchi, T. Yanagida, *Nat. Cell Biol.* **2002**, *4*, 790.
- [35] V. Belyy, M. A. Schlager, H. Foster, A. E. Reimer, A. P. Carter, A. Yildiz, *Nat. Cell Biol.* **2016**, DOI 10.1038/ncb3393.
- [36] J. E. Cronan, *J. Biol. Chem.* **1990**, *265*, 10327.
- [37] K. D. Whitley, M. J. Comstock, Y. R. Chemla, *High-Resolution Optical Tweezers Combined With Single-Molecule Confocal Microscopy*, Elsevier Inc., **2017**.
- [38] M. P. Landry, P. M. McCall, Z. Qi, Y. R. Chemla, *Biophys. J.* **2009**, *97*, 2128.
- [39] M. Swoboda, J. Henig, H. M. Cheng, D. Brugger, D. Haltrich, N. Plumeré, M. Schlierf, *ACS Nano* **2012**, *6*, 6364.

- [40] M. D. Wang, H. Yin, R. Landick, J. Gelles, S. M. Block, *Biophys. J.* **1997**, *72*, 1335.
- [41] J. Camunas-Soler, M. Ribezzi-Crivellari, F. Ritort, *Annu. Rev. Biophys.* **2016**, *45*, 65.
- [42] H. Kasai, N. Iwamoto-Tanaka, S. Fukada, *Carcinogenesis* **1998**, *19*, 1459.
- [43] R. Roy, S. Hohng, T. Ha, *Nat. Methods* **2008**, *5*, 507.
- [44] J. Y. Tinevez, N. Perry, J. Schindelin, G. M. Hoopes, G. D. Reynolds, E. Laplantine, S. Y. Bednarek, S. L. Shorte, K. W. Eliceiri, *Methods* **2017**, *115*, 80.
- [45] J. Schindelin, I. Arganda-Carreras, E. Frise, V. Kaynig, M. Longair, T. Pietzsch, S. Preibisch, C. Rueden, S. Saalfeld, B. Schmid, J. Y. Tinevez, D. J. White, V. Hartenstein, K. Eliceiri, P. Tomancak, A. Cardona, *Nat. Methods* **2012**, *9*, 676.